CHAPTER 5

VIRTUAL CATHODE FORMATION MECHANISM IN THE RELTRON*

*Part of this work has been communicated as:

Manpuran Mahto and Pradip Kumar Jain, "Virtual Cathode Formation Mechanism study in the Reltron Oscillator," *IEEE Transactions on Electron Devices* (under review).

VIRTUAL CATHODE FORMATION MECHANISM IN THE RELTRON

5.1. Introduction

High power microwave (HPM) sources have been aroused considerable research interests in the last few decades due to HPM emerging applications. These HPM sources include both conventional microwave tubes in the relativistic regime as well as specialized HPM devices. The use of intense relativistic electron beam (IREB) has significantly enhanced the RF output power of the conventional devices. Relativistic klystron, relativistic magnetron, and relativistic backward wave oscillators are few such devices in the slow wave category. The IREB gyrotron and free electron laser (FEL) are in the fast wave category. Virtual cathode oscillator (vircator) is a popular HPM device; however, its efficiency is rather low. Also, vircator high output impedance value makes RF output coupling difficult with the load. Magnetically insulated line oscillator (MILO) is a compact HPM source capable of generating gigawatts of power, but it suffers from the problem of pulse shortening as well as the requirement of additional mode converter to couple the RF power with the external antenna [Benford *et al.* (2007)].

In this chapter, the virtual cathode formation in the reltron oscillator is described. The analytical study of space charge limiting current, RF electric field in steady state condition and beam wave interaction mechanism during reltron operation are presented. The space charge limiting current responsible for the virtual cathode formation is estimated by extending the approach used for the relativistic klystrons [Friedman *et al*. (1988)]. Then, the RF electric field distribution under the steady state of this virtual cathode condition is obtained utilizing the Millar's approach [Miller

(1982), Jiang *et al*. (1995)]. The vircator analysis of Jiang *et al*. [Jiang *et al*. (2001)] is used here to demonstrate the virtual cathode formation in the different cavities section of the reltron device. The virtual cathode formation mechanism is also demonstrated using PIC simulation with the underlying the concept behind this phenomenon.

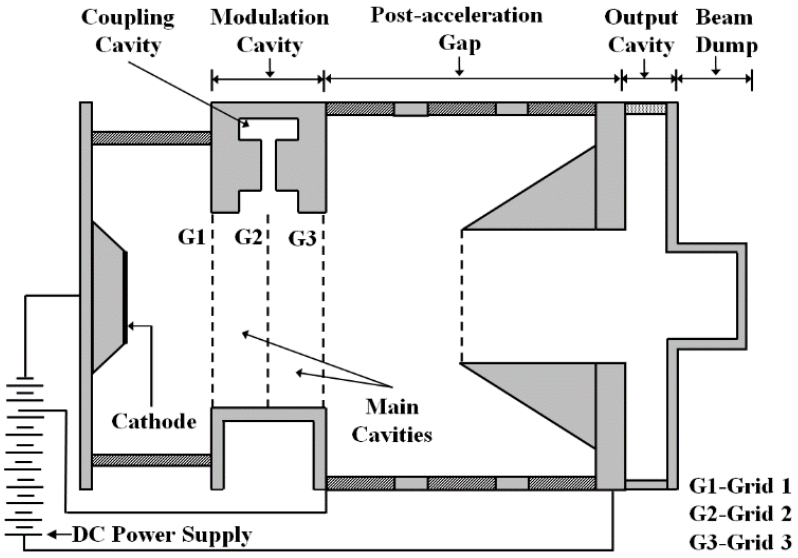

Figure 5.1: Basic schematic diagram of a reltron.

5.2. Analysis

In the reltron oscillator, a high DC pulsed voltage is applied between the cathode and the modulation cavity to excite the electrons via explosive emission process. This process creates a plasma layer on the cathode surface, and it is assumed to be stationary in nature initially. But due to the application of high DC potential in the device, transient electromagnetic (EM) waves are excited which perturbs the plasma. The perturbed plasma oscillates at the plasma frequency and results in the generation of intense relativistic electron beam (IREB) current. When these high current electron beams enter into the modulation cavity, they interact with the EM waves resulting in the generation of space charge waves. The modulating cavity is a side coupled cavity

structure, which consists of two main cavities and a coupling cavity which connects to the main cavities through a coupling slot. The modulating cavity operates in the TM_{01} mode and the three grids placed in its back, middle and front, allow the passage of electrons while confining the radial space charge electric field between the metal grid boundaries (Fig. 5.1). Due to the presence of high saturated electric field and rapid growth rate, the beam current approaches the space charge limiting current. As a consequence, the potential of the propagating electron beam is depressed, and they do not move forward. This creates a negative potential well known as a virtual cathode.

5.2.1. Space Charge Limiting Current

In reltron, the IREB currents lie close to the space charge limiting current and the self-magnetic field developed in the device is sufficiently high to propagate the electrons only in the longitudinal direction. At this point, the potential depression starts, and the kinetic energy drops to $\gamma = \gamma_0^{1/3}$. In this situation, using the convective derivative on the axial beam velocity governed by the Lorentz force equation gives the relation as [Friedman *et al*. (1988)]:

$$\gamma^3 \left(\frac{\partial}{\partial t} + v \frac{\partial}{\partial z} \right) v = \frac{e}{m} E\{z,t\} \ , \tag{5.1}$$

where *e* and *m* are the electron charge and mass at rest, respectively, $E\{z,t\}$ is the axial space charge electric field and $\gamma (= (1 - v^2 / c^2)^{-1/2})$ is the relativistic mass factor. The terms *v* and *c* represent the electron beam velocity and the speed of the light, respectively.

The surface density of the beam $\sigma\{z,t\}$ can be obtained by using the continuity equation as [Friedman *et al*. (1988)]:

$$\frac{\partial \sigma\{z,t\}}{\partial t} + \frac{\partial}{\partial z}(v\,\sigma\{z,t\}) = 0\,. \tag{5.2}$$

From Maxwell's Faraday law with the perfect conductor boundary conditions under the assumption of long wave approximation, the differential equation can be obtained as [Friedman *et al*. (1988)]:

$$-\frac{\varepsilon_0}{r_c \ln(r_m / r_c)}\frac{\partial E\{z,t\}}{\partial z} = \left(\frac{\partial^2}{\partial z} - \frac{1}{c^2}\frac{\partial^2}{\partial t^2}\right)\sigma\{z,t\}\,, \tag{5.3}$$

where ε_0 is the permittivity of the free space, r_c is the radius of the cathode and r_m is the radius of the main cavities. The axial electric field $E\{z,t\}$ in the expression (5.1) will induce a current limitation phenomenon known as space charge limiting current, and in the steady state condition $(\partial / \partial t = 0)$, expression (5.1) becomes:

$$\gamma^3 v\frac{\partial v}{\partial z} = c^2\frac{\partial \gamma}{\partial z} = \frac{e}{m}E\{z,t\} = -\frac{e}{m}\frac{\partial \phi}{\partial z}\,. \tag{5.4}$$

where the term ϕ is the electrostatic potential. As the electron propagates through the RF modulation cavity, the kinetic energy of the electron beam is converted into the potential energy, and from conservation of energy, we have the relation:

$$\gamma mc^2 + e\phi = \gamma_{inj} mc^2 \tag{5.5}$$

where γ_{inj} is the relativistic mass factor at the first grid injection position, G1, in Fig. 5.1. From conservation of charge the product of the beam surface density and axial beam velocity becomes constant, *i.e.*:

$$\sigma v = const \ , \tag{5.6}$$

and the beam surface density is defined by:

$$\sigma = \frac{\varepsilon_0}{r_c \ln(r_m / r_c)} \phi \ . \tag{5.7}$$

Combining equations (5.5), (5.6) and (5.7) we can simplify the relationship as:

$$\gamma_{inj} = \gamma + \frac{I_0}{I_s \beta} \ , \tag{5.8}$$

where I_0 is the initial beam current at the cathode surface, and β is the RF phase propagation constant. The normalized threshold current (I_s) is the current developed in the cavity before the space charge potential is set up and it is defined as:

$$I_s = \frac{2\pi\varepsilon_0 mc^3}{e \ln(r_m / r_c)} \ . \tag{5.9}$$

From (5.5) and (5.8), it can be observed that the kinetic energy of the electrons reduces as the IREB current increases and the largest permissible current known as space charge limiting current (I_{sc}) is given by:

$$I_{sc} = \frac{8.5(\gamma_{inj}^{2/3} - 1)^{3/2}}{\ln(r_m / r_c)} kA = I_s (\gamma_{inj}^{2/3} - 1)^{3/2} kA \ . \tag{5.10}$$

When the IREB current reaches to a critical current value, the self-magnetic field thus produced becomes sufficient to establish the electron beam insulation condition. This IREB current further exceeds and reaches to the space charge limiting current value. Under this condition, the electron flow stops and the electrons cloud act as a virtual cathode. Thereafter, incident electrons split into two sets: (i) transmitted electrons which

cross the virtual cathode, and (ii) reflected electrons which propagate in the reverse direction towards the physical cathode.

5.2.2. Steady State Condition

In the steady state condition, the total current density is the sum of the transmitted and reflected current densities, where the term *n* represents the electron density. The electrons propagate in the longitudinal direction and the electric field ($E\{z,t\} = -d\phi / dz$) developed due to the space charge waves can be expressed in terms of the electron density using Poisson equation as [Möller (2012)]:

$$\frac{dE\{z,t\}}{dz} = -\frac{d^2\phi}{dz^2} = -\frac{\sigma\{z,t\}}{\varepsilon_0}. \tag{5.11}$$

In view of $j = -\sigma v = -nev$, the above expression can be rewritten as:

$$dE\{z,t\} = -\frac{j}{\varepsilon_0 v} dz = -\frac{j}{\varepsilon_0 v} \frac{d\phi}{E\{z,t\}}$$

$$\Rightarrow \quad \frac{\varepsilon_0 E\{z,t\}}{j} dE\{z,t\} = -\frac{1}{v} d\phi. \tag{5.12}$$

Integrating equation (5.12) and solving yields:

$$E\{z,t\} = \sqrt{-\frac{2Jmc}{e\varepsilon_0}} (\gamma^2 - 1)^{1/4}. \tag{5.13}$$

The above expression represents the electric field profile between the injection position and the virtual cathode. The electric field becomes null at the virtual cathode when the boundary condition $E(\phi = -V_0) = 0$ is applied. The time required to reach the electrons

from the virtual cathode to the injection position is known as the time of flight or transit time τ which can be found as:

$$\tau = \int_0^{\tau} dt = -\int_{z_{VC}}^{0} \frac{dz}{v} = -\int_{z_{VC}}^{0} \frac{en}{j} dz = \int_0^{E(0)} \frac{\varepsilon_0}{j} dE\{z,t\} \ , \tag{5.14}$$

where z_{vc} is the position of the virtual cathode in the longitudinal direction. Solving equation (5.14), transit time τ can be written as:

$$\tau = \sqrt{\frac{2\varepsilon_0 m\gamma}{ne^2}} = \frac{\sqrt{2}}{\omega_p}. \tag{5.15}$$

Here $\omega_p = (ne^2 / \varepsilon_0 m\gamma)^{1/2}$ is the plasma frequency. Here in expression (15), τ denotes the time required by the electrons to reach the injection position from the virtual cathode, also known as the electron flight time and is inversely proportional to the plasma frequency [Miller (1982,) Jiang *et al*. (2001)].

5.2.3. Interaction Process

The modulation cavity of the reltron contains three grids (Fig. 5.1), and therefore there is a possibility of formation of multiple virtual cathodes. Therefore, the virtual cathode formation in the reltron oscillator becomes a complex process in which two stages of virtual cathodes are formed in the system. In the first stage, two virtual cathodes are formed simultaneously while in the second stage only one virtual cathode is formed. The basic mechanism of formation of the virtual cathode in the reltron oscillator is shown in Fig. 5.2. The virtual cathodes are formed due to the potential depression of electrons, in which some of the electrons are reflected back towards the real cathode, and due to the cathode potential, they have reflected again towards the

virtual cathode. These reflected electrons also take part in the modulation process. In case of multiple virtual cathodes formation, electrons oscillate in between the virtual cathodes. The overall process of virtual cathode formation becomes very complicated in nature and becomes very difficult to show the formation of the virtual cathode in reltron analytically. Therefore, we assume that the virtual cathode is already formed in the system and proceed further to analyze the RF wave interaction mechanism [Dubinov *et at*. (2004), Champeaux *et at*. (2015), Champeaux *et at*. (2016), Shao *et at*. (2009)].

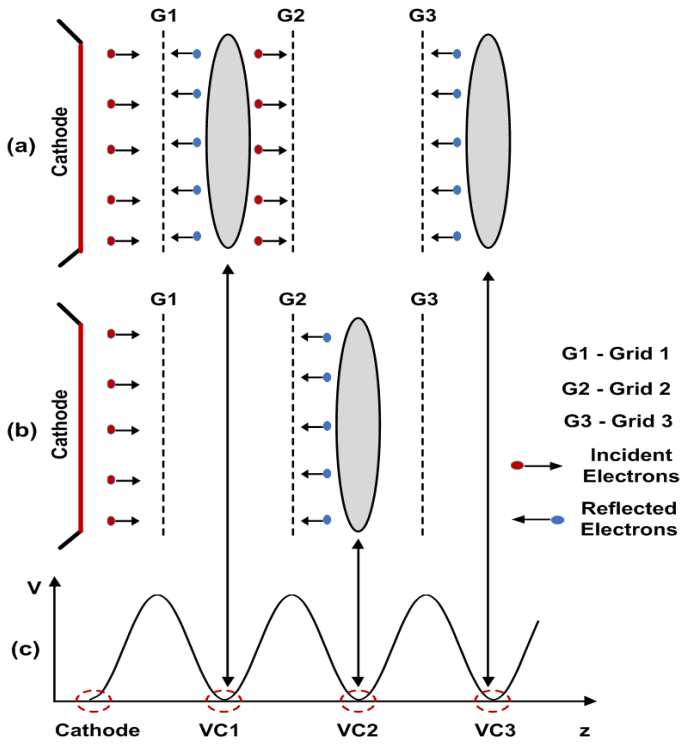

Figure 5.2: Behaviour of the virtual cathode in reltron (a) double virtual cathode condition, (b) single virtual cathode condition (c) axis representation.

Consider the case when two virtual cathodes are formed, simultaneously as shown in Fig. 5.2(a). One virtual cathode (VC1) is formed in the first grid spacing (*i.e.* after the first grid G1) and the second virtual cathode (VC3) is formed in the post-acceleration region (*i.e*. after the third grid G3). The RF electric field generated due to the beam space charge can be expressed as:

$$E_{mc} = E_0 \sin \omega t \,, \tag{5.16}$$

where E_0 represents the peak field amplitude of the beam space charge field.

Initially, we analyze the virtual cathode VC1 and this virtual cathode (VC1) will exert an oscillating electric field on the intense relativistic electron beam. The oscillating electric field due to the virtual cathode VC1 can be represented as:

$$E_{VC1} = E_0' \sin \omega t \,, \tag{5.17}$$

where E_0' is the peak field amplitude due to VC1. The net momentum p is given by the RF electric field and oscillating electric field of VC1 as:

$$\frac{dp}{dt} = e(E_0 + E_0') \sin \omega t \,.$$

Suppose the incident electrons enter the injection point (first grid G1), at time t_0 and as it propagates to the virtual cathode VC1, the kinetic energy of the electrons start decreasing. After some time $t = t_0 + \tau_1$, the electrons reach at the virtual cathode VC1 where its velocity drop to zero; then we can represent the relation for the injected electrons as [Jiang *et al*. (2001)]:

$$p_{i1} = \int_{t_0}^{t_0+\tau_1} e(E_0 + E_0') \sin \omega t dt \tag{5.18}$$

$$\Rightarrow p_{i1} = -\frac{e(E_0 + E_0')}{\omega} [\cos \omega(t_0 + \tau_1) - \cos \omega t_0] \,.$$

Solving the above expression provides:

$$p_{i1} = \frac{2e(E_0 + E_0')}{\omega} \sin \omega \left(t_0 + \frac{\tau_1}{2} \right) \times \sin \omega \left(\frac{\tau_1}{2} \right). \tag{5.19}$$

The reflected electrons from the virtual cathode VC1 will reach the injection position G1 at a particular time $t = t_0 + \tau_1 + \tau_2$; then the electron momentum can be expressed as [Jiang *et al*. (2001)]:

$$p_{r1} = \int_{t_0+\tau_1}^{t_0+\tau_1+\tau_2} e(E_0 + E_0')\sin\omega t dt \tag{5.20}$$

$$\Rightarrow p_{r1} = -\frac{e(E_0 + E_0')}{\omega}[\cos\omega(t_0 + \tau_1 + \tau_2) - \cos\omega(t_0 + \tau_1)].$$

The above expression can be written in the form:

$$p_{r1} = \frac{2e(E_0 + E_0')}{\omega}\sin\omega\left(t_0 + \tau_1 + \frac{\tau_2}{2}\right)\times\sin\omega\left(\frac{\tau_2}{2}\right). \tag{5.21}$$

The average momentum in the cavity is the difference between the momentums caused by the incident electrons (p_{i1}) and reflected electrons (p_{r1}) and it can be determined by:

$$p_{av1} = \frac{\overline{p_{i1} - p_{r1}}}{p_{i1}} = \frac{2e(E_0 + E_0')}{\omega T p_{i1}}\int_0^T \left[\begin{array}{l}\sin\omega\left(t_0 + \frac{\tau_1}{2}\right)\times\sin\omega\left(\frac{\tau_1}{2}\right) - \\ \sin\omega\left(t_0 + \tau_1 + \frac{\tau_2}{2}\right)\times\sin\omega\left(\frac{\tau_2}{2}\right)\end{array}\right] dt_0, \tag{5.22}$$

where $T(=2\pi/\omega)$ is the oscillation period. The average momentum (p_{av1}) is due to the interaction between the oscillating electric field and intense relativistic electron beam.

Suppose, the transit time of the electron does not depend on the direction of propagation, then $\tau' = \tau_1 = \tau_2$ and the above expression can be rewritten as:

$$p_{av1} = \frac{2e(E_0 + E_0')}{\omega T p_i}\int_0^T \left[\sin\omega\left(t_0 + \frac{\tau'}{2}\right) - \sin\omega\left(t_0 + \frac{3\tau'}{2}\right)\right]\times\sin\omega\left(\frac{\tau'}{2}\right) dt_0. \tag{5.23}$$

If the derivative of the time of flight with respect to its average value can be represented as $\delta_1 = \tau' - \bar{\tau}$, then equation (5.23) can be written as:

$$p_{av1} = -\frac{4e(E_0 + E_0')}{\omega T p_{i1}} \int_0^T \left[\sin^2 \omega \left(\frac{\bar{\tau} + \delta_1}{2} \right) \times \cos \omega \left(t_0 + \bar{\tau} + \delta_1 \right) \right] dt_0 \ . \tag{5.24}$$

Expression (5.18) can be modified in the form:

$$p_{i1} = e(\bar{\tau} + \delta_1) E_{mc} + e \int_{t_0}^{t_0 + \tau} eE_0' \sin \omega t dt \ . \tag{5.25}$$

If the incident momentum is represented as $p_{i1} = e\bar{\tau}E_{mc}$, then expression (5.25) provides the relation:

$$\omega \delta_1 = -2 \frac{E_0'}{E_{mc}} \sin \omega \left(\frac{\bar{\tau}}{2} \right) \sin \omega \left(t_0 + \frac{\bar{\tau}}{2} \right). \tag{5.26}$$

When the phase shift is very less, *i.e.*, $\delta_1 << \bar{\tau}$ then the amplitude of the oscillation becomes also very low and in this situation expression (5.23) can be modified as:

$$p_{av1} = -\frac{e(E_0 + E_0')}{\omega T \ p_{i1}} \int_0^T \left[\omega \delta_1 \times \sin \omega \bar{\tau} \times \cos \omega \left(t_0 + \bar{\tau} \right) \right] dt_0 \, . \tag{5.27}$$

Substituting (5.26) in (5.27) and solving yields:

$$p_{av1} = \left(\frac{E_0'}{E_{mc}} \right)^2 F\{\omega \bar{\tau}\} \quad . \tag{5.28}$$

The amplitude of the oscillating electric field is very high, and therefore, the function $F\{\omega \bar{\tau}\}$ is defined as:

$$F\{\bar{\omega\tau}\} = -\frac{1}{\bar{\omega\tau}}\sin^2\left(\frac{\bar{\omega\tau}}{2}\right)\sin\bar{\omega\tau} \tag{5.29}$$

From (5.28) and (5.29) it can be observed that when $F\{\bar{\omega\tau}\} < 0$, the electron takes energy from the RF field otherwise a reverse operation takes place. Further, the oscillating electric field double folds the electron RF energy exchange, and it is proportional to the square of E_0' / E_{mc}.

Consider the situation when the phase shift becomes large enough, then the amplitude of modulation can be saturated, or it may reduce if the electron phase is over-shifted. This can deviate the dependency of the beam RF energy exchange from the intensity of the oscillating electric field, particularly for higher values of E_0' / E_{mc}. For this situation consider the notations:

$$s_1 = \bar{\omega\tau},\ A_1 = \frac{E_0'}{E_{mc}},\ \theta = \omega t_0\ . \tag{5.30}$$

Using the notations mentioned in (5.30) and substituting (5.26) in (5.24) provides the relation:

$$p_{av1} = -\frac{2A_1}{s_1\pi}\int_0^{2\pi}\left[\begin{array}{l}\sin^2\left(\frac{s_1}{2} - A_1\sin\left(\frac{s_1}{2}\right)\sin\left(\theta+\frac{s_1}{2}\right)\right)\times \\ \cos\left(\theta + s_1 - 2A_1\sin\left(\frac{s_1}{2}\right)\sin\left(\theta+\frac{s_1}{2}\right)\right)\end{array}\right]d\theta\,. \tag{5.31}$$

The above expression provides the net momentum due to the formation of the virtual cathode VC1.

Now, we analyze the effect of second virtual cathode VC3 as shown in Fig. 5.2(a). The virtual cathode (VC3) will also exert an oscillating electric field on the

intense relativistic electron beam, propagating towards the virtual cathode VC3. The oscillating electric field of VC3 can be represented as:

$$E_{VC3} = E_0'' \sin \omega t \,, \tag{5.32}$$

where E_0'' is the peak field amplitude due to the oscillating electric field of VC3.

Suppose the incident electrons from VC1 starts at a time $t = t_0 + \tau_1$ and reach the VC3 at time $t = t_0 + \tau_1 + \tau_3$, where the velocity of the electrons again drops to zeros and we can represent the momentum of the injected electrons as:

$$p_{i2} = \int_{t_0+\tau_1}^{t_0+\tau_1+\tau_3} e(E_0 + E_0'') \sin \omega t dt \tag{5.33}$$

$$\Rightarrow p_{i2} = -\frac{e(E_0 + E_0'')}{\omega} [\cos \omega(t_0 + \tau_1 + \tau_3) - \cos \omega(t_0 + \tau_1)] .$$

Solving the above yields:

$$p_{i2} = \frac{2e(E_0 + E_0'')}{\omega} \sin \omega\left(t_0 + \tau_1 + \frac{\tau_3}{2} \right) \times \sin \omega\left(\frac{\tau_3}{2} \right). \tag{5.34}$$

If the reflected electrons from VC3 reach to VC1 at a particular time $t = t_0 + \tau_1 + \tau_3 + \tau_4$, then the momentum of the reflected electrons can be represented as:

$$p_{r2} = \int_{t_0+\tau_1+\tau_3}^{t_0+\tau_1+\tau_3+\tau_4} e(E_0 + E_0'') \sin \omega t dt \tag{5.35}$$

$$\Rightarrow p_{r2} = -\frac{e(E_0 + E_0'')}{\omega} [\cos \omega(t_0 + \tau_1 + \tau_3 + \tau_4) - \cos \omega(t_0 + \tau_1 + \tau_3)] \quad .$$

The above expression can be expressed in the form:

$$p_{r2} = \frac{2e(E_0 + E_0'')}{\omega} \sin\omega\left(t_0 + \tau_1 + \tau_3 + \frac{\tau_4}{2}\right) \sin\omega\left(\frac{\tau_4}{2}\right). \quad (5.36)$$

The average momentum due to the virtual cathode VC3 is determined by the momentums caused by the incident electrons (p_{i2}) and reflected electrons (p_{r2}) as:

$$p_{av2} = \frac{\overline{p_{i2} - p_{r2}}}{p_{i2}} = \frac{2e(E_0 + E_0'')}{\omega T p_{i2}} \int_0^T \left[\begin{array}{l} \sin\omega\left(t_0 + \tau_1 + \frac{\tau_3}{2}\right) \times \sin\omega\left(\frac{\tau_3}{2}\right) - \\ \sin\omega\left(t_0 + \tau_1 + \tau_3 + \frac{\tau_4}{2}\right) \times \sin\omega\left(\frac{\tau_4}{2}\right) \end{array} \right] dt_0 . \quad (5.37)$$

It is again assumed that the transit time of the electrons between VC1 and VC3, does not depend on the direction of propagation, than $\tau'' = \tau_3 = \tau_4$. The above expression can be modified as:

$$p_{av2} = \frac{2e(E_0 + E_0'')}{\omega T p_{i2}} \int_0^T \left[\sin\omega\left(t_0 + \tau' + \frac{\tau''}{2}\right) - \sin\omega\left(t_0 + \tau' + \frac{3\tau''}{2}\right) \right] \times \sin\omega\left(\frac{\tau''}{2}\right) dt_0 . \quad (5.38)$$

The derivative of the time of flight with respect to its average value can be represented as $\delta_2 = \tau'' - \bar{\tau}$, then equation (5.38) can be written as:

$$p_{av2} = \frac{2e(E_0 + E_0'')}{\omega T p_{i2}} \int_0^T \left[\sin\omega\left(t_0 + \tau' + \frac{\tau''}{2}\right) - \sin\omega\left(t_0 + \tau' + \frac{3\tau''}{2}\right) \right] \times \sin\omega\left(\frac{\tau''}{2}\right) dt_0 . \quad (5.39)$$

Expression (5.33) can be rewritten as:

$$p_{i2} = e(\bar{\tau} + \delta_2) E_{mc} + e\int_{t_0+\tau_1}^{t_0+\tau_1+\tau_3} eE_0'' \sin\omega t dt \quad . \quad (5.40)$$

If the incident momentum from the virtual cathode VC1 is expressed as $p_{i2} = e\bar{\tau}E_{mc}$, then equation (5.40) provides the relation:

$$\omega\delta_2 = -2\frac{E_0''}{E_{mc}}\sin\omega\left(\frac{\bar{\bar{\tau}}}{2}\right)\sin\omega\left(t_0+\bar{\tau}+\frac{\bar{\bar{\tau}}}{2}\right). \tag{5.41}$$

Substituting (5.41) in (5.39) provides the relation:

$$p_{av2} = -\frac{2A_2}{s_1\pi}\int_0^{2\pi}\left[\begin{array}{l}\sin^2\left(\frac{s_2}{2}-A_2\sin\left(\frac{s_2}{2}\right)\sin\left(\theta+s_1+\frac{s_2}{2}\right)\right)\times \\ \cos\left(\theta+s_1+s_2-2A_1\sin\left(\frac{s_1}{2}\right)\sin\left(\theta+\frac{s_1}{2}\right)\right) \\ -2A_2\sin\left(\frac{s_2}{2}\right)\sin\left(\theta+s_1+\frac{s_2}{2}\right)\end{array}\right]d\theta. \tag{5.42}$$

Here, the notations are represented as: $s_2 = \omega\bar{\bar{\tau}}$, and $A_2 = E_0''/E_{mc}$. The above expression deals with the momentum when the two virtual cathodes VC1 and VC2 are formed simultaneously as shown in Fig. 5.2(a). When a single virtual cathodes VC2 is formed in the cavity as shown in Fig. 5.2(b), the condition will be similar to the expression (5.31). This two stage virtual cathode formation is periodic in nature which occurs one after another.

5.3. Device Modeling

When a high DC potential is applied to the cathode, the axial electric fields are generated. As the work function of the potential energy exceeds the work of the cathode, electron emission starts through the explosive emission process. Due to the explosive emission process, the cathode surface is covered with the plasma layer and a consequence of it, the intense relativistic electron beam (IREB) is generated, and a large current flows along the longitudinal direction. The relativistic electron beam propagates through the RF interaction structure (*i.e.*, modulation cavity) where it gets synchronized

with space charge waves, and the beam starts decelerating. This reduction in the kinetic energy of the electrons is transferred to the RF field. As soon as, the beam current approaches the space charge limiting current, electron beam propagation stops leading to the virtual cathode formation in the reltron device.

Due to the formation of the virtual cathode, some of the electrons reflect back, and these reflected electrons are again propagated in the forward direction under the positive electric gradients and reach to the successive cavities. Since, reltron contains three metal grids (G1, G2, and G3 in Fig.1) in the modulating cavity, create the possibility of simultaneous formation of the multiple virtual cathodes. Thereby making the virtual cathode formation a complicated process and its understanding becomes necessary to understand the device behavior. To understand the physical phenomena behind it, particle-in cell (PIC) simulation can be very helpful. In order to visualize the dynamics of virtual cathode in reltron CST PS has been used.

To perform the PIC simulation of the reltron oscillator, a typical experimental reltron oscillator reported by Miller *et al*. [Miller *et al*. (1994)] is selected, and its electrical parameter is listed in Table 5.1. First of all the reltron structure is designed according to the device design methodology described in Chapter 3, and then the structure is modeled as per the material properties, electrical and structural parameters. The various design parameters considered in the process of PIC simulation are as follows: cathode radius: 15 mm, anode-cathode gap (along the z-axis): 20.50 mm, radius of the main cavity: 38.27 mm, radius of the coupling cavity: 25.51 mm, radius of the idler: 12.75 mm, the distance between the grids (grid spacing along the z-axis): 18.70 mm, post-acceleration gap (along the z-axis): 53.30 mm, drift tube length: 44.80 mm. Here, the critical parameters are grid spacing (distance between the two grids) and the anode-cathode gap through which the device performance can be controlled. If the

anode-cathode gap distance is much larger than the spacing between the two consecutive grids than the current developed in the modulation cavity is very less and unable to establish the self-magnetic insulation condition. And if the anode cathode-gap distance is much smaller than the spacing between the two consecutive grids than the virtual cathode formation does not take place. Both these situations degrade the device performance. For the better performance, the anode-cathode gap is generally kept at 1.1 times the grid spacing. This optimized length is calculated by Miller *et al*. [Miller *et al*. (1992)] through various experiments. Another parameter which should be taken care is drift tube cut-off frequency. In the extraction waveguide, the slow space charge waves having the positive group velocity move in the forward direction through which RF can be extracted while the slow space charge waves having the negative group velocity moves in the backward direction. To avoid this backward propagation, the drift tube of the device should be kept below the device oscillation frequency to avoid this reverse propagation. Since within a few wavelength, the waves attenuate, therefore, the drift tube length is kept long to prevent this backward wave propagation.

Table 5.1: Device Beam Parameters [Miller *et al*. (1994)]

Specifications	**Values**
Operating frequency	2.75 GHz
Beam Current	1000 A
Total beam voltage	950 kV
Cathode voltage	200 kV
Post-acceleration voltage	750 kV

5.4. Result and Discussion

Reltron oscillator is a klystron type of HPM device which uses a side-coupled modulation cavity where the dominant interaction between RF waves and electrons take place. This modulation cavity contains two main axial cavities separated by three metal grids G1, G2, and G3, as shown in Fig. 5.1. These metal grids help in the virtual cathode formation which in turn produces an intense electron bunching. In this section, the space charge limiting current responsible for the generation of virtual cathode, RF beam energy exchange mechanism and behaviour of RF interaction process in the presence of electron beam is computationally appreciated using the analysis developed in section 5.2. The results obtained through the PIC simulation is also discussed.

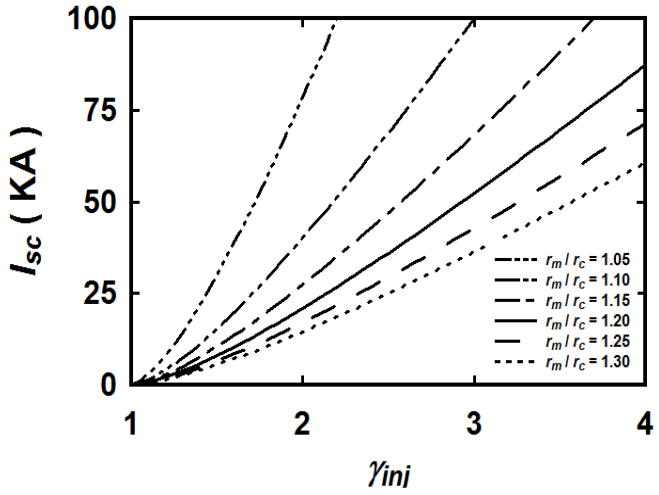

Figure 5.3: Plot of space charge limiting current (I_{sc}) versus γ_{inj} for different main cavity to cathode radii ratio r_m/r_c.

5.4.1. Analytical Results

The purpose of this study is to find the necessary conditions for the generation and propagation of the bunched intense relativistic electron beam. The main issue with an efficient propagation of intense relativistic electron beam is the creation of negative

potential well (known as virtual cathode) which generates due to the beam space charge. At a particular injection energy, a maximum beam space charge current *i.e.*, space charge liming current can flow in the device, and it depends on the beam impedance. Using expression (5.10), the space charge limiting current is computed and is plotted in Fig. 5.3, as a function of the relativistic mass factor at the beam injection position γ_{inj} for different values of the main cavity to cathode radii ratio r_m/r_c. To get a space charge limiting current, the electron drift energy should reach a value of $\gamma_{inj}^{1/3}$. From Fig. 5.3, it can be observed that the beam spread in γ_{inj} decreases as the ratios r_m/r_c increases until all the particles attain the same velocity. The reason behind the phenomenon is that the beam is surrounded by the electrostatic field which acts as a major role in the total RF energy available in the cavity. The impedance of the cavity is not affected more when the beam is away from the tube wall, and in this situation, the drift energy becomes much less than the injected energy.

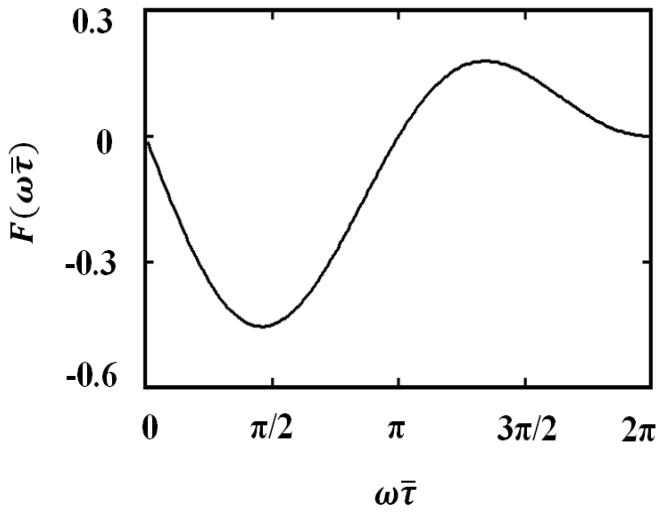

Figure 5.4: Plot of the function $F\{\omega\bar{\tau}\}$ versus phase angle $(\omega\bar{\tau})$ which is proportional to the average momentum of the electron beam.

When the virtual cathode is formed, the beam-RF energy exchange becomes proportional to $(E_0' / E_{mc})^2$. It is due to the oscillating electric field of the virtual cathodes which performs in two ways: (i) current modulation of the reflected electrons and (ii) RF energy is to be extracted from these current modulated electrons. To demonstrate a phase relationship between the field and the electron momentum a relationship between the function $F\{\omega\bar{\tau}\}$ versus the phase angle $(\omega\bar{\tau})$ is shown in Fig. 5.4. When the function $F\{\omega\bar{\tau}\}$ lies in the negative half cycle, the electron momentum becomes in phase, to lose energy from the beam, *i. e.*, energy transfer is from electron beam to the field. When it lies in the positive half cycle, the electron momentum is in phase to gain the energy from the field, *i.e.*, the energy transfer is from field to the electron beam. The minimum point of the function $F\{\omega\bar{\tau}\}$ is the optimum operating point of the RF generation by the reltron oscillator. From Fig. 5.4, it can be seen that a minimum negative amplitude is obtained at ~π/2.

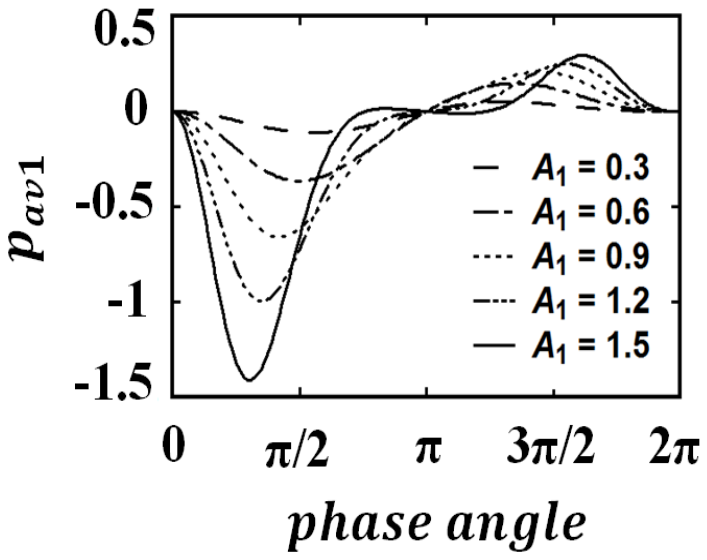

Figure 5.5: Plot of average momentum (p_{av1}) versus phase angle $(s_1 = \omega\bar{\tau})$ for different value of $A_1 (= E_0' / E_{mc})$.

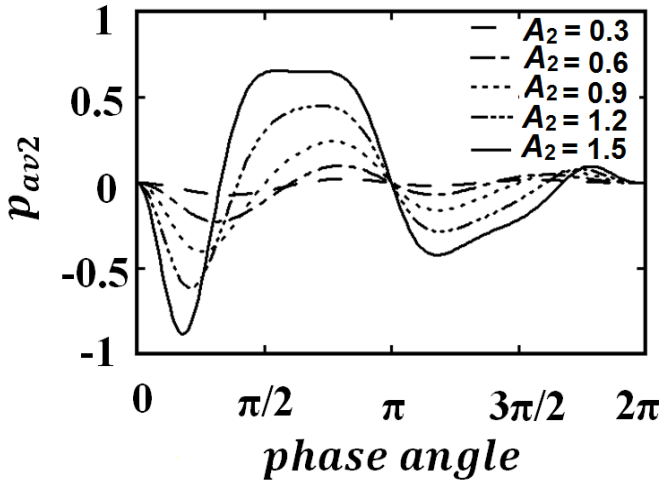

Figure 5.6: Plot of average momentum (p_{av2}) versus phase angle ($s_2 = \omega\bar{\tau}$) for different value of $A_2 (= E_0'' / E_{mc})$.

To investigate the behaviour of RF interaction process during the formation of the virtual cathode in reltron, a relationship between the average momentums and phase angles from expressions (5.31) and (5.42) are plotted in Fig. 5.5 and Fig. 5.6, respectively. In Fig. 5.5, a single negative minima is obtained indicating the formation of single virtual cathode, while in Fig. 5.6 two negative minima indicate the double virtual cathode formation in the reltron oscillator. The formation of the single and double virtual cathode in the reltron oscillator is periodic in nature. This is achieved by performing the numerical integration of the expressions (5.31) and (5.42) for different values of A_1 (= 0.3, 0.6, 0.9, 1.2, 1.5) and A_2 (= 0.3, 0.6, 0.9, 1.2, 1.5), respectively. From Fig. 5.5 and Fig. 5.6, it can be observed that the depth of the average momentum increases for higher values of the magnitude A_1 and A_2. This indicates that at a higher level of field amplitudes, the electron momentum generated by the beam space charge around the virtual cathode in the reltron increases. This will enhance the feedback of RF waves in virtual cathode which results in improved microwave efficiency in the reltron oscillator.

5.4.2. PIC Simulation Results

To get an insight information of the virtual cathode formation process in reltron oscillator, a commercial particle-in-cell (PIC) code ‘‘CST Particle Studio” is reconfigured to simulate the reltron device. At first, in the absence of electron beam, the side-coupled modulation cavity is simulated using Eigenmode solver to ensure the operating mode and resonating frequency. After ensuring the desired resonating frequency and mode excitation in the device structure, the complete structure of the device is modeled. The beam parameters used for the device simulation is listed in Table 5.1.

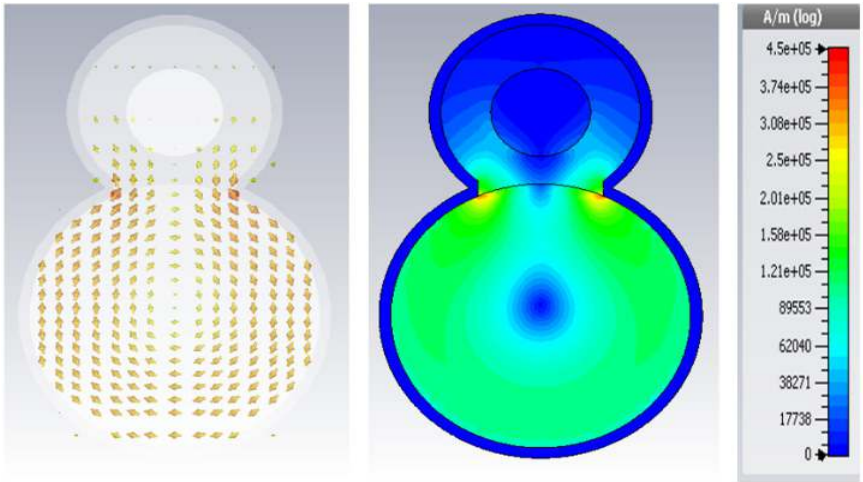

Figure 5.7: TM_{01} mode of operation in the side coupled modulation cavity (a) vector plot, (b) contour plot.

To study the electromagnetic behaviour and operating mode in the side-coupled modulation cavity, RF cavity simulation is carried out using CST Eigenmode Solver in the absence of electron beam. Considering the reltron structure as of a perfect metal, the tangential electric field is set as null (E_t = 0) in all the metal boundary, and the

background material is kept as normal (vacuum). Figs. 5.7 (a) and (b) show the vector and contour plots of the magnetic field profile. From Fig. 5.7, it can be observed that the device is operating in the desired TM_{01} mode.

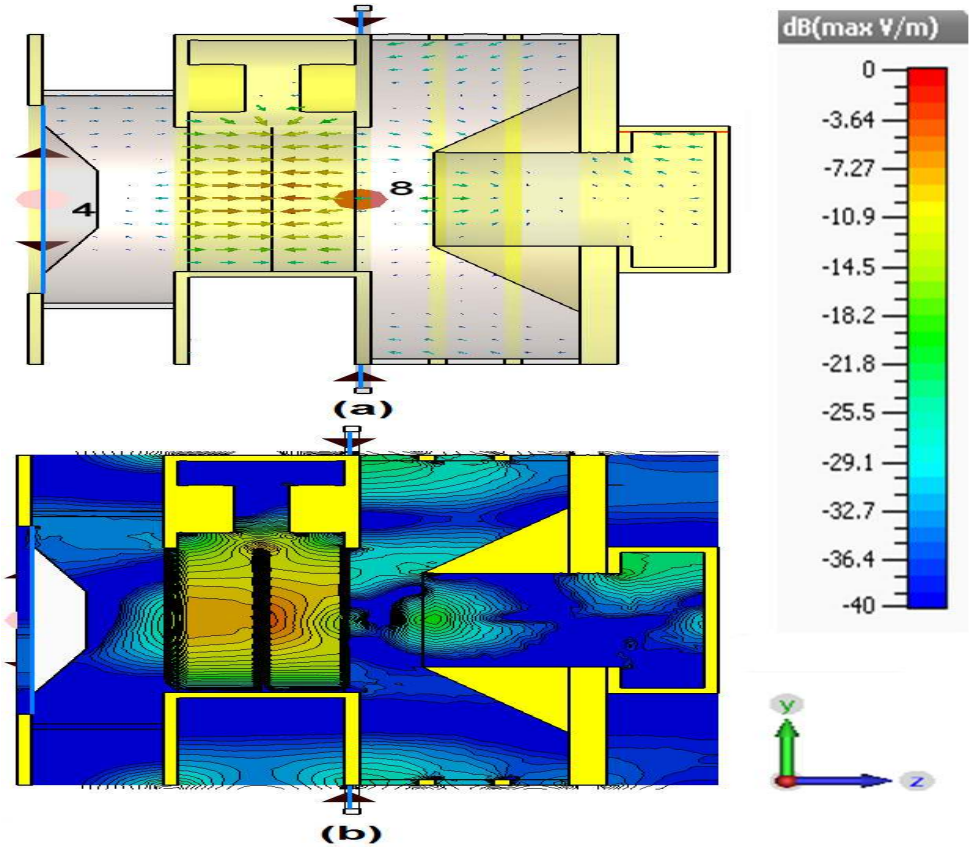

Figure 5.8: Electric field distribution in the reltron oscillator (a) vector plot (b) contour plot.

To investigate the electron beam and RF interaction behaviour and understand the virtual cathode formation in the device PIC simulation of the device is made reconfiguring a commercial PIC code "CST Particle Studio". An experimental reltron device [Miller *et al.* (1994)] is modeled as per the parameters given in section 5.3. Discrete ports are used as a voltage source to provide the accelerating potential to the device and a total DC potential of 950 kV is applied for the PIC simulation. This DC potential is distributed at two places: (i) one at the cathode surface with 200 kV and (ii)

another at the post-acceleration gap with 750 kV, both for 100ns time duration with 1ns rise time. The cathode is annular in shape and acts as a particle source in the reltron oscillator. The explosive electron emission model is chosen for the electron emission with an initial beam current of 1000 A. Despite of having very low initial beam current than the space charge limiting current, and it is self-sufficient to emit the electrons along with initial cathode voltage. The reltron output cavity is modeled with the waveguide port to extract the RF output power. With these parameters, the PIC simulation is carried out for 100 ns duration.

The vector and contour plot of the spatial electric field distribution in the y-z plane radiated at 2.75 GHz is shown in Fig. 5.8. Here, from Fig. 5.8(a), it can be observed that the electric field in the main cavities of the modulation cavity oscillate in the opposite polarity, while the coupling cavity does not contain any electric field. This is the desired and resonating $\pi/2$-mode condition. The contour plot is also plotted in Fig. 5.8(b), which indicates the intense electric field distribution in the main cavities.

To explore the behaviour of the electron's trajectory, the phase space obtained during the particle simulation is shown in Fig. 5.9. It indicates the energy exchange mechanism between the electron and RF wave at different instant of time. The electron's kinetic energy distribution at 3.3 ns is shown in Fig. 5.9 (a). Here, it can be observed that the electrons are emitted from the cathode and propagate through the modulation cavity. At this moment the electrons reach out to the extraction cavity without any back reflection of electrons. After some time when the oscillation gets build up the space charge forces come into existence, and due to the Lorenz reversal force, some of the electrons starts reflecting in the backward direction as shown in Fig. 5.9 (b) at 4.9 ns. Further, as the oscillation becomes strong enough the virtual cathode formation takes place, and the reflection of electrons in the reverse direction becomes

more frequent as shown in Fig. 5.9 (c) at 11.1 ns. These reflected electrons also help in the modulation process which results in the intense electron bunches as shown in Fig. 5.9 (d) at 11.3 ns.

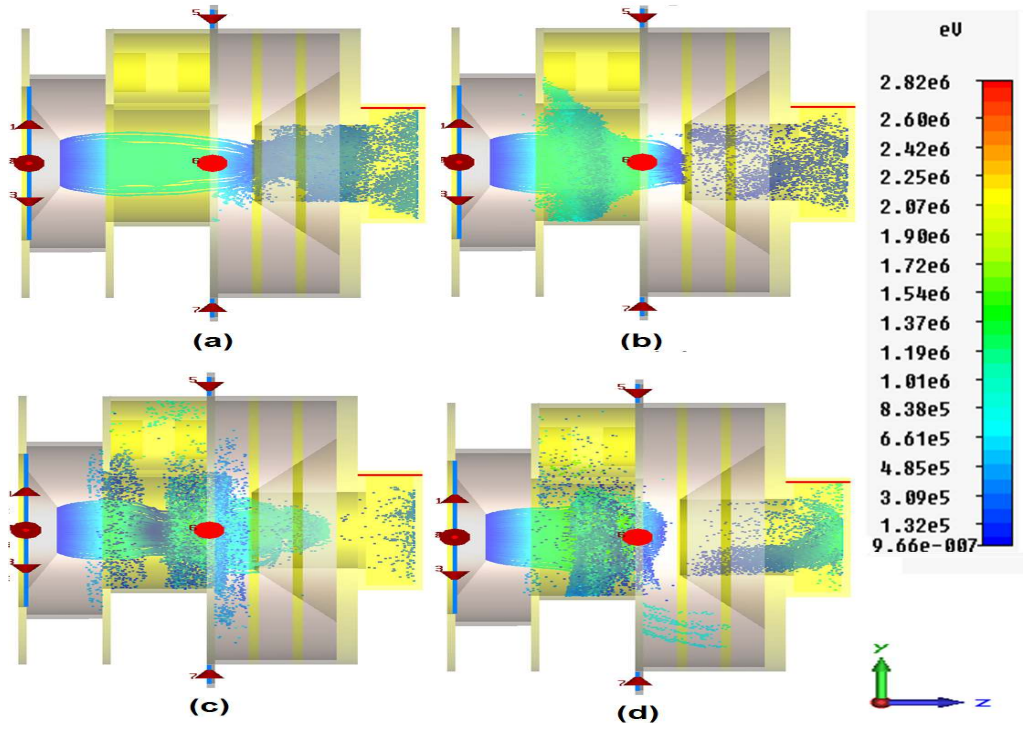

Figure 5.9: Plot of electrons phase space at (a) 3.3 ns (b) 4.9 ns (c) 11.1 ns (d) 11.3 ns time duration.

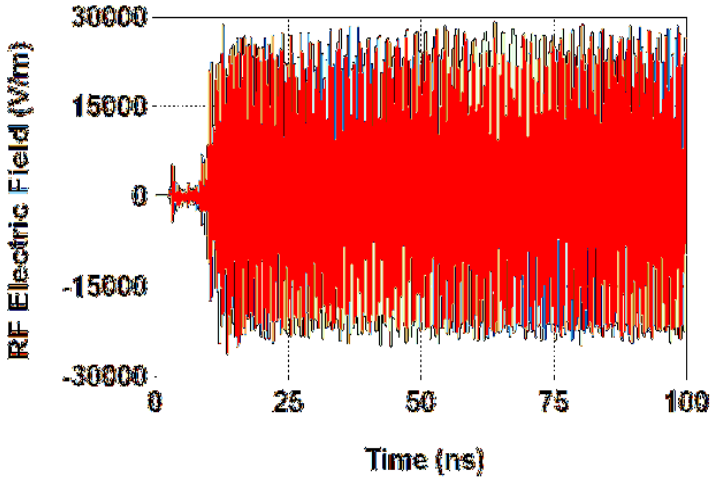

Figure 5.10: Plot of RF electric field developed at the extraction port.

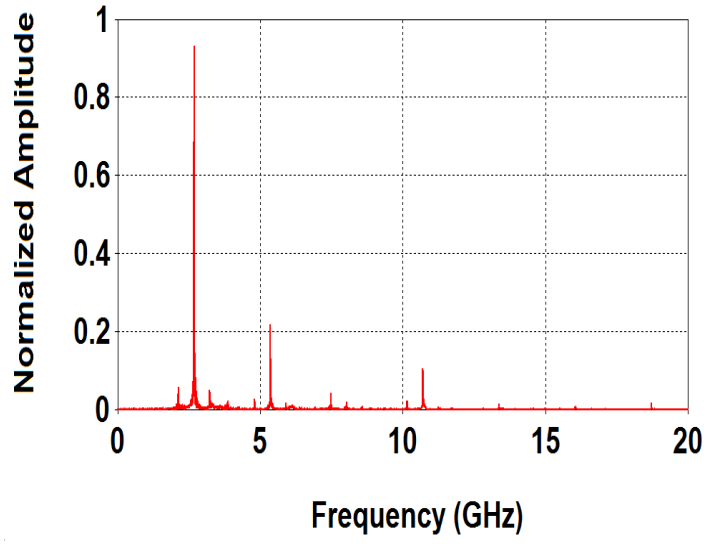

Figure 5.11: Plot of the device oscillation frequency spectrum.

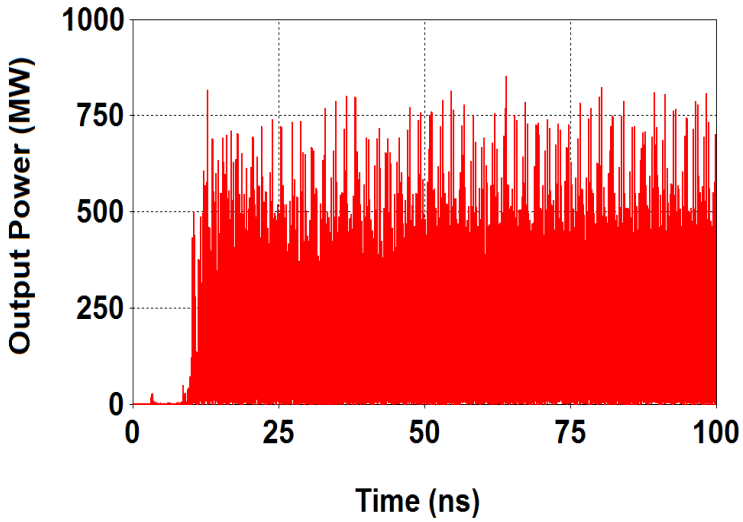

Figure 5.12: Plot of RF power developed at the extraction port.

After the particle simulation is carried out for the 100 ns duration, with beam parameters listed in Table 5.1, the RF electric field is obtained using a waveguide port in the extraction cavity, is plotted in Fig. 5.10. A plot oscillation frequency spectrum is shown in Fig. 5.11, which is obtained using the Fast Fourier transform (FFT) method. It indicates that the device oscillation frequency is ~ 2.75 GHz. The temporal RF power developed at extraction cavity for the beam parameters: beam current = 1000 A (applied

at the cathode), dc beam voltage = 200 KV (applied at the cathode) and the post-acceleration voltage = 750 KV (applied between the modulation cavity and the extraction cavity, *i. e.*, post-acceleration region) as mentioned in Table I, is depicted in Fig. 5.12. It indicates that with these given parameters the particle simulation generated ~ 435 MW RF output power with an efficiency of ~ 46%. These particle simulations results are in agreement of ~ 9% with the reported experimental results of Miller *et al.* [Miller *et al.* (1994)].

The modulation cavity consists of three metal grids named as G1, G2, and G3 as shown in Fig. 5.1 which can be visualized as the equivalent of a multistage vircator [Champeaux *et at*. (2015), Champeaux *et at*. (2016)], however, the operating mechanism is somewhat different. The electron beam coming out from the annular cathode via explosive electron emission process is pre-modulated while passing the first grid G1 and forms a periodic dispersion mechanism propagating through the second metal grid G2. The electrons crossing the third metal grid G3 enter into the post-acceleration region maintaining the bunch-dispersion cycle unchanged. The beam wave interaction process takes place in the modulation cavity in which the electrons are modulated once in the first main cavity (between G1 and G2) and again modulated in the second main cavity (between G2 and G3). This dual-stage modulation process creates intense electron bunches. Since the electrons carry the negative charge with them, so these propagating space charge give additional potential to the electron beam. As a result, the potential energy becomes much higher than the kinetic energy and a deep negative potential well is created and electron bunch stops propagating further. This results in the formation of the virtual cathode formation [Shao *et at*. (2009)].

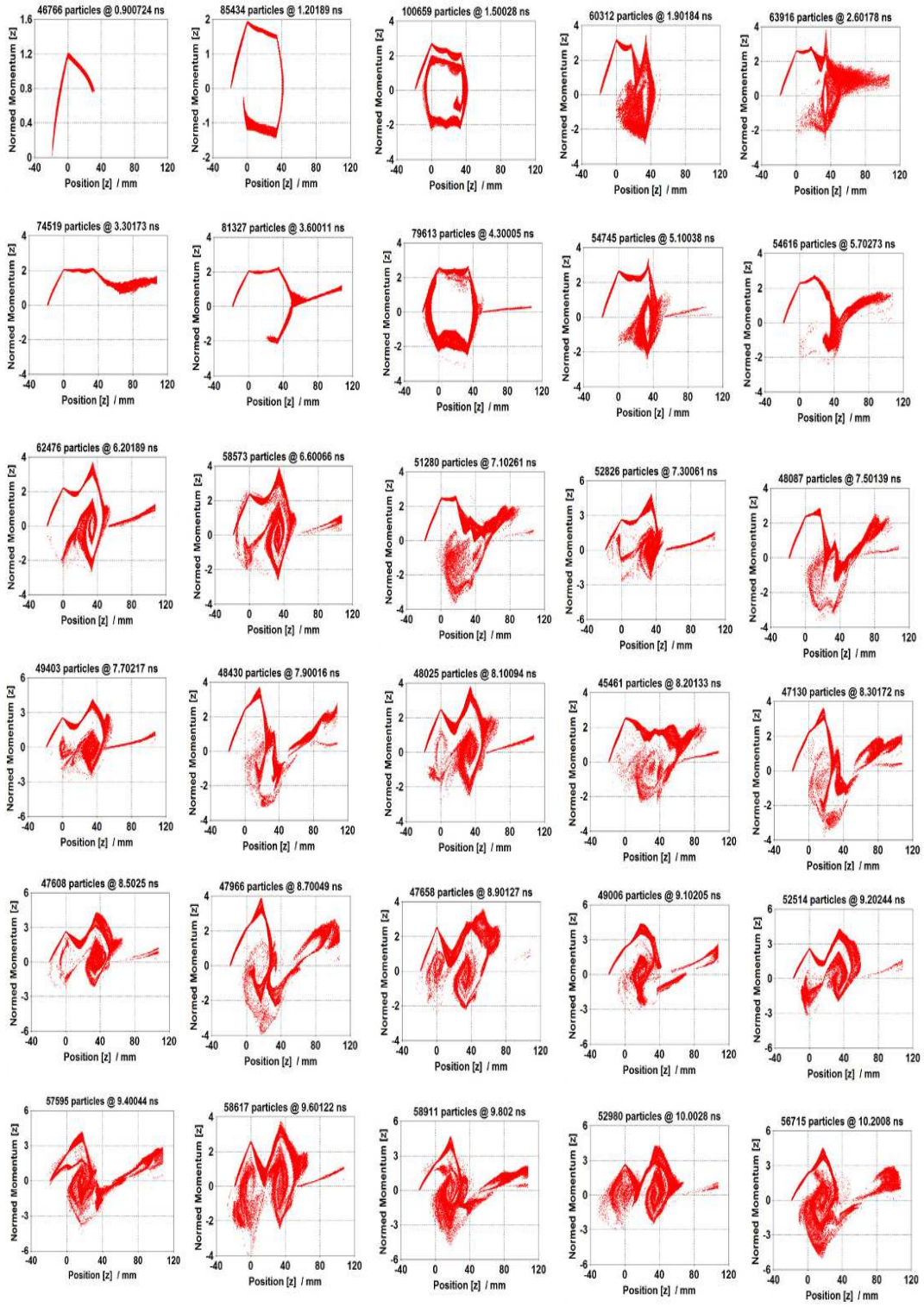

Figure 5.13: Plot of electron's momentum to visualize the process of virtual cathode formation in the reltron oscillator at different instant of time before the saturation of oscillation. In the present device the three metal grids (G1, G2, and G3 as shown in Fig. 5.1) are at the positions 0 mm, 18.70 mm and 37.40 mm, respectively, along the longitudinal direction.

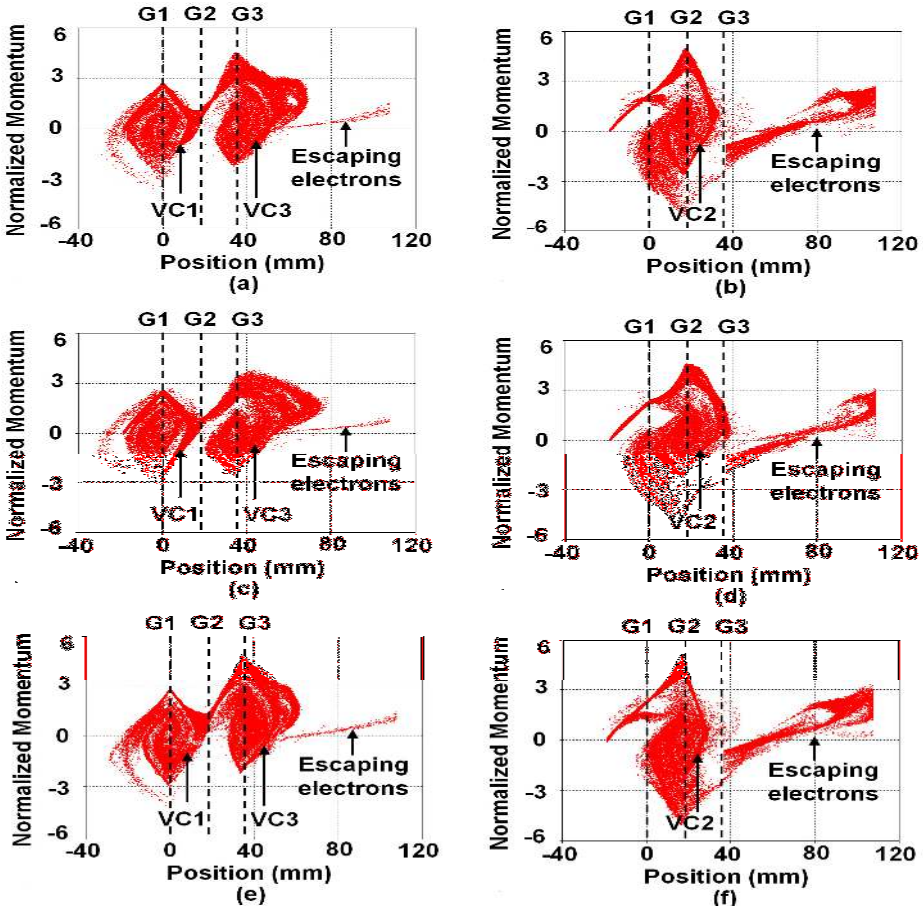

Figure 5.14: Plot of electron's normalized momentum at (a) 11.1 ns (b) 11.3 ns (c) 11.5 ns (d) 11.7 ns (e) 49.6 ns (f) 49.8 ns.

The formation of the virtual cathode in the reltron oscillator is depicted in Fig. 5.13 at different instant of time before the saturation of the oscillation in the device. Here in the present device the three metal grids G1, G2, and G3 are at the positions 0.00 mm, 18.70 mm and 37.40 mm, respectively. Initially, at 3.3 ns, the virtual cathode does not form, and the electrons can propagate to the extraction cavity unaffected. After some time at 6.6 ns due to the increase in the space charge forces, the virtual cathodes start appearing in the device. At later times 10 ns and 10.2 ns the virtual cathodes are clearly visible and are in the way to get stable. Fig. 5.14 indicates the phase space momentum after the saturation of oscillation. In this situation, the current modulation of electrons reaches upto 100% under the optimum condition. The virtual cathode

formation mechanism in the reltron is different from the vircator in which two stages of virtual cathodes are formed. In the first half cycle, two virtual cathodes are formed simultaneously, one after the first grid G1 (virtual cathode VC1) and second after the third grid G3 (virtual cathode VC3) as shown in Fig. 5.14 (a) at 11.1 ns. Then in the second half cycle, these two virtual cathodes disappear, and a new virtual cathode is formed after the second grid G2 (virtual cathode VC2) as shown in Fig. 5.14 (b) at 11.3 ns.

At the grids, the velocity of the electrons is maximum, and it starts reducing as electrons propagate towards the virtual cathode. The space charge continues to grow after the formation of the virtual cathode, and at a higher level, it stops the electrons. As a result, the virtual cathode comes closer to the grid until the kinetic energy of the electrons become high enough to pass through the virtual cathode. In this situation, the virtual cathode is disturbed, and the electrons propagate towards the extraction cavity. This phenomenon can be seen as escaping electrons in Fig. 5.14. Thereafter, the new virtual cathodes are formed again after the space charge potential is set up. The virtual cathode formation in the reltron is a periodic process in which single and double virtual cathodes are formed alternately. One such instance is shown in Fig. 5.14 (c) and Fig. 5.14 (d) at 11.5 ns and 11.7 ns duration, respectively, and another at later time 49.6 ns and 49.8 ns is shown in Fig. 5.14 (e) and Fig. 5.14 (f), respectively. This periodic virtual cathode formation process in the reltron sets up oscillation, thereby the RF radiation. The electrons reflections between the virtual cathode and physical cathode also support the RF radiation. It is not necessary that oscillation frequency of the device, virtual cathode, and reflecting electrons have the same frequency. However, for optimum interaction, all these three should be forced to oscillate at the same frequency.

The necessary condition for the formation of virtual cathode is that the momentum of the electrons become negative due the potential depression. The analytical description in Section II predicted the formation of two stage virtual cathodes formation and similar phenomenon has also been observed through PIC simulation. Initially, the virtual cathode VC3 is formed (as can be seen from Figs. 2 and 8) and due to the reflection of the electrons another virtual cathode VC1 gets formed. Once the oscillation get established in the device, these virtual cathodes (VC1 and VC3) form simultaneously. When the kinetic energy of the electrons become sufficiency high the virtual cathode VC3 is disturbed while the virtual cathode VC1 shifts to the position of VC2. After that the virtual cathode VC2 get shifted to the position of virtual cathode VC3 and a new virtual cathode forms at the position of VC1. This process is periodic in nature and movement of IREB electrons to and forth direction in the modulation cavity significantly enhances the electron beam bunching, which in turn responsible for the improvement of the device efficiency and increase in the RF power output of the device.

5.5. Conclusion

An analytical study is presented here to demonstrate the virtual cathode formation mechanism in the reltron oscillator. The space charge liming current developed in the modulating cavity of the device is demonstrated with the help of the relativistic klystron theory. The vircator analysis is extended here to demonstrate the RF interaction mechanism due to the formation of virtual cathode in the reltron device. The analysis predicted that two stages of the virtual cathode are formed in reltron. In the first stage, only one virtual cathode is formed while in the second stage two virtual cathodes are formed simultaneously, and thereafter it alternates. PIC simulation of an HPM

source – reltron, using and reconfiguring a commercial PIC code, has been demonstrated to investigate the electron beam and RF wave interaction, and the virtual cathode formation mechanism during its operation. The mode of operation of the side-coupled modulation cavity is confirmed as TM_{01}. Through PIC simulation, two stages periodic formation of the virtual cathode have been shown in the reltron. In one instant double virtual cathodes are formed, in which one has appeared after the first grid and another after the third grid. In the second instant, only one virtual cathode is generated after the second grid. The virtual cathode formation in the reltron is a periodic process. The device oscillation frequency is appeared at ~ 2.75 GHz. Further, the performance of the device is also studied which showed that with a total current of 1000 A, cathode voltage of 200 kV and post-acceleration voltage of 750 kV, the developed RF power is ~ 435 MW. The total efficiency of the device is ~ 46 %, and the particle simulation results are in agreement of ~ 9% with the experimentally reported results. The results obtained through PIC simulation study about the virtual cathode formation during the operation of the reltron operation corroborates our analytical findings reported in the previous paper in this journal. It is hoped that the present study would greatly help the high power microwave tube developers.